RSC Advances

PAPER

View Article Online
View Journal | View Issue

Cite this: *RSC Adv.*, 2025, **15**, 3331

Glass fiber treated with a glycine bridged silane coupling agent reinforcing polyamide 6(PA6): effect of hydrogen bonding

Dinghua Yu, *[ab] Jianqiang Wang[b] and Guowei Wang[b]

Silane coupling agents play an indispensable role in improving interfacial adhesion of composite materials, but their interaction mechanism is often unclear. This article combines experiments and theoretical calculations to reveal the importance of hydrogen bonds between silane coupling agents and the matrix polyamide 6 in improving the mechanical properties of composite materials. Firstly, glycine bridged silane (GBSilane) was synthesized and the structure was confirmed by FT-IR, ^{1}H NMR and HRMS. Secondly, with glass fiber treated using GBSilane as a filler, the mechanical properties of glass fiber/PA6 composite materials were studied. Compared with untreated glass fiber/PA6 composites, under the optimal treatment concentration of 1.5%, the tensile strength of glass fiber/PA6 composites treated with 3-aminopropyl triethoxysilane (APTES) and GBSilane increased by 41% and 67%, respectively, and the notch impact strength increased by 55% and 96.5%, respectively. Lastly, density functional theory (DFT) calculations revealed that stronger hydrogen bonds have formed between GBSilane and PA6 than APTES, which have induced the stronger PA6–GBSilane binding energy of 58.20 kJ mol^{-1}. By comparison, the binding energy of PA6–APTES is only 30.91 kJ mol^{-1}. These results demonstrated that the as-synthesized GBSilane could improve the mechanical properties of PA6 composites through an enhanced hydrogen bonding mechanism.

Received 28th October 2024
Accepted 28th January 2025

DOI: 10.1039/d4ra07680j

rsc.li/rsc-advances

Introduction

Since the 1940's, the emergence of composite materials with excellent performance can be considered a milestone event in the history of materials science development. As the largest category of composite materials, fiber-reinforced polymers (FRP) have witnessed tremendous progress in modern civilization because of their ease of processing, corrosion resistance, light weight, high strength and cost-effectiveness.[1] Reinforcing fibers, including glass fiber,[2] carbon fiber,[3] renewable fiber,[4] *etc.*, are used as the load-bearing element, and the polymers are used as the continuous phase or matrix, which could not only protect and disperse fibers, but also transfer loads. The commonly used matrix materials are divided into two categories, that is thermosetting materials,[5] such as unsaturated resins, epoxy resins, and polyurethane resins, and thermoplastic materials[6] such as polyamide, polycarbonate, polystyrene, PVC, PP, *etc.* Although FRP have been applied in engineering for 80 years, they could be still seen in rapidly developing fields at present such as lightweight electric vehicles,[7] electrical insulators in ultra high voltage power transmission,[8] wind turbine blades,[9] liquid hydrogen storage,[10] high railway,[11] drones,[12] *etc.*

The macroscopic properties of fiber-reinforced polymers not only depend on the chemical constituents and physical structure of fibers and polymers, but also depend on the interface state between matrix resin and reinforcing fibers, including interface composition, bonding mode, and bonding strength.[13] The interface between the fiber and matrix is crucial to the performance of the composite, which plays a role in smoothly transferring the stress borne by the matrix material to the reinforced fiber structure.[14] Therefore, improving the interface bonding strength is an important consideration in designing high-performance composite materials. In order to improve interface bonding, researchers have optimized interface properties from different perspectives. The first attempt is depositing nanomaterials such as graphene, graphene oxide and carbon nanotubes, on fiber surfaces, improving the interfacial bonding strength through the size effect of nanomaterials. Chen *et al.*[15,16] reported that the carbon fiber surface was modified by silanized graphene nanosheets through liquid phase deposition, and the modified carbon fiber was used to reinforce the epoxy resin matrix. The gradient interphase of graphene nanosheets on the carbon fibers has induced carbon fiber–epoxy composite flexural improvement including strength by 15% and modulus by 16%, respectively. Feng *et al.*[17] have grafted carbon nanotubes onto carbon fibers, and the as-

[a]*Ningbo Polytechnic China Light Industry Plastic Mold Engineering Technology Research Center, Ningbo, 315800, PR China*
[b]*College of Biotechnology and Pharmaceutical Engineering, Nanjing Tech University, Nanjing 211816, PR China. E-mail: yudh@njtech.edu.cn; Tel: +86-25-58139386*

resulted modified fibers with hierarchical structure were used to reinforce the polyamide matrix. The carbon nanotubes deposition could improve the fiber surface roughness and wettability to polyamide, which led to a 35% increase in impact strength. Kumar *et al.*[18] have deposited cellulose nanocrystals onto glass fibers, and the as-prepared hierarchical glass fibers were used to reinforce the epoxy resin. The results demonstrated that the introduced ~300 nm interphase had improved the mechanical properties including a 30% increase in the interlaminar shear strength and a 43% increase in flexural strength.

Although the hierarchical interphase through nanomaterials deposition on reinforcement fibers can improve their mechanical properties to a certain extent, which could be mainly beneficial from mechanical bonding between fibers and matrix at the mesoscopic scale, the additional interphase may increase the possibility of interlayer delamination, ultimately leading to material failure. Natural materials have provided researchers with new ideas on how to optimize the interface bonding strength at a more microscopic level.[19,20] Jia *et al.*[21,22] utilized bio-mimic hydrogen bond concept to optimize material interface and reported the improved mechanical properties of carbon fiber–epoxy resin composite materials. In their reports, the organic–inorganic hybrid materials including hyperbranched polyamide-amine (HPAA) and graphene oxide (GO) were successively deposited onto the surface of carbon fibers. The high hydrogen bond density from HPAA has promoted graphene oxide deposition on carbon fibers and interaction between hierarchical carbon fibers and epoxy resin matrix. Comparing with carbon fiber without modification, the modified HPAA–GO/carbon fiber could obviously improve impressive strength of 94.5% and 110.0% in respective interfacial strength and fracture toughness.

The above literature results indicate that in order to construct critical interfacial phases, not only hierarchical surface roughness should be considered, but also chemical bonds, electrostatic interactions, hydrogen bonds, *etc.* should also be considered. Interestingly, in natural composite materials such as teeth and bones, there are extensive hydrogen bond interaction[23] between nano-fibrils and nano-sized hydroxyapatites, which could contribute to toughening mechanisms including intrinsic plasticity, extrinsic crack bridging, and deflection for simultaneous strength and toughness.[24–26] However, in artificial composite materials, the construction of hydrogen bonds has not been given much attention, and there are no reports on whether the use of hydrogen bonds can improve the mechanical properties of materials.

In long-term practice, silane coupling agents have always been a key material for composite materials, which can not only protect the fibers from wear, but also improve the adhesion between reinforcement fibers and polymer matrix, thereby achieving the goal of improving the performance of composite materials.[27] Developing new silane coupling agents to further improve the performance of composite materials is of great significance, both in theoretical research and in practical applications. Therefore, in this paper, glycine bridged silane coupling agent (GBSilane) was synthesized and the structure was confirmed through spectroscopic methods such as FT-IR, ^{1}H NMR, HRMS, *etc.* It was further used to treat the surface of glass fibers through chemical bonding linkage and the modified glass fibers were used to reinforce PA6 matrix materials. In order to further disclose the interaction mechanism, density functional theory was used to simulate the hydrogen bond interaction between silane coupling agents and PA6.

Experimental

Materials

Glycine, thionyl chloride ($SOCl_2$), methanol (MEOH), triethylamine (Et_3N), dichloromethane (DCM), tetrahydrofuran (THF), ethylenediamine, 3-aminopropyl triethoxysilane (APTES) and 3-isocyanatopropyl triethoxysilane (IPTES) were all purchased from Shanghai Aladdin Reagent Co. without further purification. E-glass fiber was gifted by China Giant Stone Group. PA6 slices were purchased from Guangdong Xinhui Meda Nylon Co., Ltd., brand: M 2500, relative viscosity 2.45, without further purification.

Methods

Synthesis of glycine bridged silane (GBSilane). As shown in Fig. 1, GBSilane was synthesized according to our previous reported methods[28–30] with minor change through the successive four step reactions.

(1) Synthesis of glycine methyl ester hydrochloride. Glycine (5.00 g) was firstly dissolved into 100 mL of methanol, and the solution was maintained at 0 °C under ice bath conditions. Then $SOCl_2$ (8.40 g) was added dropwise, and the mixture was reacted at 25 °C for 12 h. The product was recovered through rotary evaporation and the successive drying. Finally, a white solid (6.53 g) was obtained.

(2) Synthesis of glycine methyl ester. Crude glycine methyl ester hydrochloride (6.53 g) was dispersed in 60 mL of dichloromethane to form a white suspension, then slightly excess triethylamine was added and the mixture was maintained to react at 25 °C for 12 h. After the reaction, the mixture was filtered and dichloromethane was used to rinse the filter cake several times. Then the crude products were recovered through vacuum distillation, which were further extracted with diethyl ether and subsequent vacuum distillation to obtain glycine methyl ester (2.36 g).

(3) Synthesis of glycinamide. Under Ar protection, glycine methyl ester (2.36 g) was dissolved into methanol, then slightly excess ethylenediamine was added for overnight reaction. After

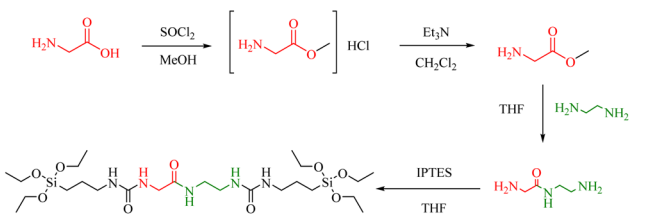

Fig. 1 The synthesis of glycine bridged silane (GBSilane).

the reaction was completed, the crude product was separated through vacuum distillation and was further purified using silica gel column chromatography. The ratio of mobile phase is MeOH : DCM : Et_3N = 10 : 1 : 1. After purification, an oily product (2.32 g) was obtained.

(4) Synthesis of glycine bridged silane (GBSilane). Under Ar protection, the oily product (2.32 g) was dissolved in 50 mL of THF, and IPTES (5.56 g) was added to the solution. The reaction was carried out at 25 °C for 12 h. After the reaction was completed, the solvent was removed by vacuum distillation, and the residue was washed with anhydrous *n*-hexane. Then the white solid product GBSilane (8.04 g) was recovered through filtration and dry. Elemental analysis, calculated for GBSilane ($C_{24}H_{53}N_5O_9Si_2$): C, 47.11; H, 8.73; N, 11.45; O, 23.53%; found: C, 47.01; H, 8.81; N, 11.52; O 23.48%.

Structure characterization of GBSilane

The elemental analysis (EA) of C, H, O and N was obtained *via* a Vario ELcube elemental analyzer with a CHNO mode. Fourier transform infrared spectrum (FT-IR) from 4000 to 400 cm^{-1} were acquired using a Vector22 Fourier Transform Infrared Spectrometer (Bruker Co., German). The sample was uniformly mixed with potassium bromide powder at a ratio of 1 : 100 and compressed into tablets. ^1H nuclear magnetic resonance spectroscopy (^1H NMR) was recorded at the AVANCE III-400 MHz spectrometer (Bruker Co., German). Tetramethylsilane (TMS) is used as the standard sample, and deuterated DMSO and $CDCl_3$ are used as solvents. The high-resolution mass spectrum (HRMS) was acquired on a MALDI-TOF mass spectrometer (Bruker Autoflex maX) with positive ion operation mode.

Surface modification of glass fiber

Glass fibers were calcined to remove surface sizing agents at 500 °C for 2 hours under air atmosphere, and the calcined glass fibers were packaged for future use. The surface modification process with APTES and GBSilane was performed according to Wei *et al.*' method with minor change.[31] APTES or GBSilane was firstly dissolved into distilled water and pH of the solution was adjusted to 4.0 with acetic acid. 100 g of calcined glass fibers were introduced to 2000 mL three necked flask, and the 1000 mL of silane solution was added. Then the mixture was heated to 70 °C and reacted for 2 h under stirring conditions. After reaction, the solid products recovered through filtration were washed with anhydrous ethanol three times, and were dried at 40 °C in a vacuum oven. The glass fibers samples modified with GBSilane were labeled as GF-GBSilane-0.5, GF-GBSilane-1.0, GF-GBSilane-1.5, and GF-GBSilane-2.0 (the numbers represent the mass percentage of silane coupling agent and glass fibers), respectively. Meanwhile, the corresponding samples treated with APTES are denoted as GF-APTES-0.5, GF-APTES-1.0, GF-APTES-1.5 and GF-APTES-2.0, respectively.

The loading amount of silane coupling agent on the surface of glass fiber was determined by thermogravimetric method, which has been performed on a STA 409 PC synchronous thermal analyzer (Netzsch, Germany). Heating rate 10 °C min^{-1}, air atmosphere, flow rate 50 mL min^{-1}. In order to reduce the influence of adsorbed water, the samples were dried at 105 °C for 2 h before experiments.

Preparation and mechanical performance of glass fiber/PA6 composite material

PA6 was firstly dehydrated and dried at 105 °C for 24 hours. Glass fiber/PA6 composite materials were prepared in a twin-screw extruder (SJSH30 type, Nanjing Rubber and Plastic Machinery Factory) under the pre-set conditions (extrusion temperature of 200–250 °C, main engine speed of 120 rpm, feeding speed of 25 rpm, granulation, vacuum drying). The addition amount of glass fiber in composite materials is uniformly 30%.

In order to determine the mechanical performances, the glass fiber/PA6 composite materials with different compositions were dried at 80 °C for 6 hours, and then were molded into standard samples through injection process (injection temperature: 240 °C; mold temperature: 60 °C) at the plastic injection machine (Rui'an Ruicheng Rubber Machinery Co., Ltd) according to ASTM D256-2010 and ASTM D638-2010. Before the operation, the spline specimens were conditioned under standard laboratory conditions (temperature: 25 ± 2 °C; relative humidity: 50 ± 5%) for 24 hours. The tensile strength was acquired at the electronic universal material testing machine (Shimadzu Corporation, Japan) according to ISO527 testing standard, and the notch impact strength was recorded at the cantilever beam impact testing machine (AJU-22, Chengde Material Testing Machine Factory) according to ISO 179 testing standard.

Density functional theory (DFT) calculations

Density functional theory (DFT) simulations were performed using Gaussian 16 program (Version B.01, Gaussian Inc. Wallingford CT, 2016).[32] In order to simplify the DFT calculations, 6-propamidohexanoic acid acetamide was used as the model repeating unit of PA6 polymer.

APTES, GBSilane, PA6 model molecule, PA6–APTES, and PA6–GBSilane were optimized with B3LYP functional and 6-311++g (d,p) basis set. All optimized structures were confirmed with no imaginary frequency.

The hydrogen bond information, including hydrogen bond length, average hydrogen bond length between PA6–APTES or PA6–GBSilane was determined. Meanwhile, energy parameters, including the electronic energy (E) and binding energy (ΔE) between single molecules and PA6–APTES or PA6–GBSilane molecules, were determined to elucidate the hydrogen bond interaction between PA6 and APTES or GBSilane.

The binding energy (ΔE, kJ mol^{-1}) of PA6–APTES or PA6–GBSilane was evaluated using the following equation:

$$\Delta E = -2625.5 \times (E_{fc} - E_f - E_c)$$

E_{fc}, E_f, and E_c are the electronic energy value of PA6–APTES/GBSilane, PA6, and APTES or GBSilane, respectively.

Results and discussion

Structural characterization of GBSilane

The infrared spectrum of the as-synthesized GBSilane is shown in Fig. 2. From the figure, the absorption peak at 3338 cm^{-1} could be attributed to the N–H stretching vibration of the amide bond, and the absorption peaks at 2975, 2935, 2885, 1442 and 1390 cm^{-1} can be related to C–H groups. Specifically, the absorption peaks at 2975, 2935 and 2885 cm^{-1} can be attributed to the symmetrical and antisymmetrical C–H stretching vibration peak of saturated carbon including CH_3– and –CH_2–, and the absorption at 1390 cm^{-1} and 1442 cm^{-1} is the characteristic peak of the bending vibration of methyl –CH_3. Obviously, the absorption at 1626 cm^{-1} could be related to the carbonyl (C=O) stretching vibration of the amide bond, and the absorption at 1581 cm^{-1} could be attributed to the deformation vibration of N–H. Additionally, the absorption at 1103 cm^{-1} and 958 cm^{-1} can be attributed to the deformation vibration of Si–O–C. Overall, these results are consistent with our previous reports.[33]

Furthermore, the as-synthesized GBSilane was analyzed by ^{1}H NMR spectroscopy, and the corresponding results are shown in Fig. 3. In our previous report,[33] serine bridged siliane has been synthesized and the assignments results of the ^{1}H NMR peaks could be used as the reference. It can be seen that the multiple peaks with a chemical shift of about 0.48 ppm represent the four hydrogen atoms of the methylene group directly connected to Si, while the triple peak at 1.1 ppm is the 18 hydrogen atoms on the methyl group in the 6 ethoxy groups. The multiple peaks at 1.35 ppm represent the four hydrogen atoms on the second carbon atom connected to Si. Obviously, the peak at 2.9 ppm represents four hydrogen atoms on the third carbon atom connected to Si, and the chemical shift at 3.0 ppm can be attributed to the two methylene hydrogen atoms between the two ureas in the middle of the molecule. Meanwhile, the chemical shift at 3.48 ppm can be attributed to the remaining methylene group adjacent to the urea group, and the peak at 3.69 ppm can be attributed to the 12 hydrogen atoms on the six methylene groups in the ethoxy group. In addition, the five peaks between 5.77–7.85 ppm represent the five hydrogen atoms connected to the amino group, and the chemical shift at 7.85 ppm belongs to the middle hydrogen atom connected to the amino group.

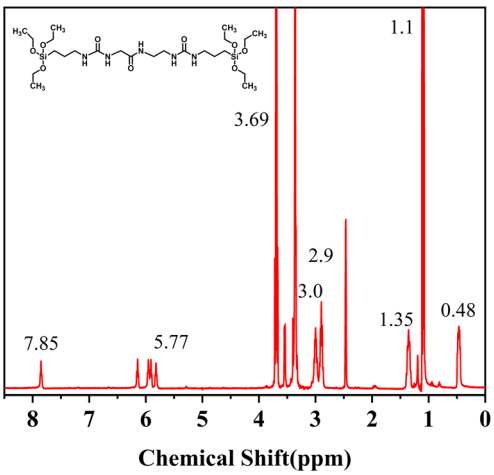

Fig. 3 The ^{1}H NMR spectrum of GBSilane.

Meanwhile, high-resolution mass spectrum of GBSilane was acquired and the corresponding results are shown in Fig. 4. From the figure, m/z = 634.3291 corresponds to the molecular ion peak (M + Na^+) of GBSilane, which is consistent with the molecular weight of the GBSilane. Overall, based on the above FT-IR, ^{1}H NMR, and HRMS results, it can be confirmed that the glycine bridged silane has been successfully synthesized.

Surface modification of glass fiber

In order to quantitatively analyze the GBSilane on the surface of glass fibers, thermogravimetric analysis was performed on modified glass fiber samples, and the corresponding results are shown in Fig. 5. It can be seen that the slight weight loss of modified glass fiber before 300 °C comes from the adsorbed water on the sample surface. For GF-GBSilane-0.5 sample, the maximum weight loss peak could be found at 383 °C. For GF-GBSilane-1.0 sample, the starting temperature of weight loss

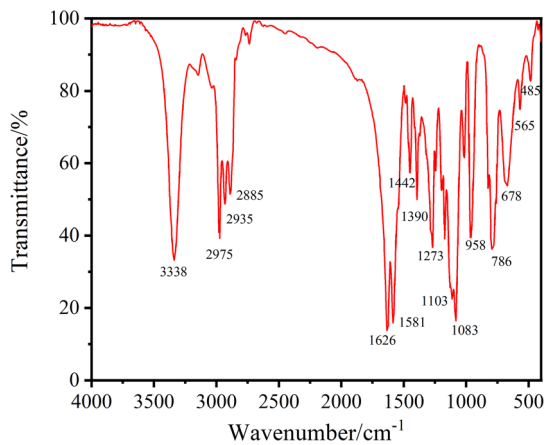

Fig. 2 The FT-IR spectrum of GBSilane.

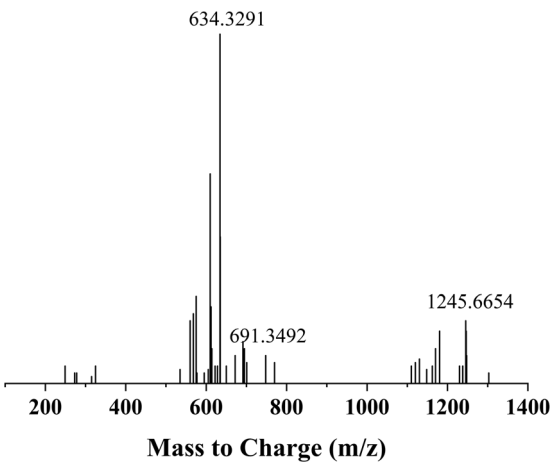

Fig. 4 The high resolution mass spectrum of GBSilane.

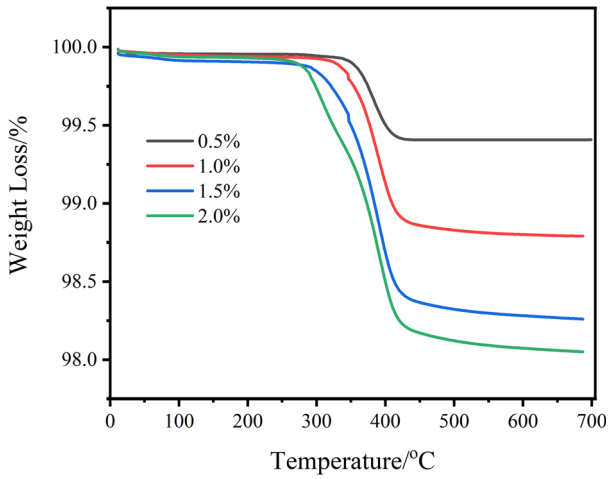

Fig. 5 The TG curves of GF-GBSilane series samples with different concentration.

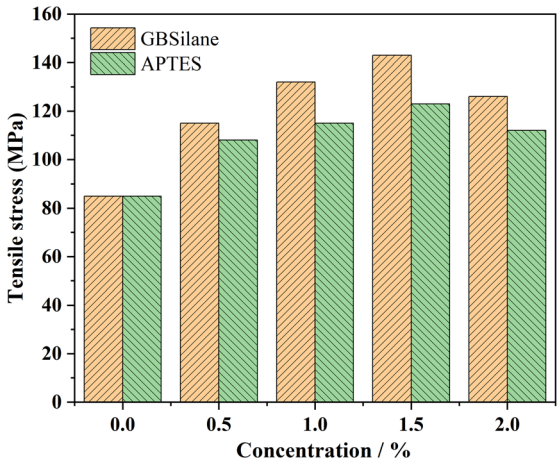

Fig. 6 Tensile stress of glass fiber/PA6 composite modified with silane coupling agent.

is 350 °C, the ending temperature of weight loss is 415 °C, and the weight loss rate is 1.02%. With the concentration increasing to 1.5% and 2.0%, the starting temperature of weight loss gradually decreases to 325 °C and 300 °C, and the ending temperature of weight loss gradually decreases to 410 °C and 405 °C, with weight loss of 1.75% and 1.9%, respectively. The above results show that the weight loss of the sample is consistent with the concentration of GBSilane, indicating that the modification process can efficiently immobilize the GBSilane on the surface of the glass fiber. On the other hand, as the concentration of GBSilane increases, the temperature of the weight loss step shifts towards lower temperatures, which could be induced by different surface state of coupling agents. Specifically, when the coupling agents amount exceeds the single-layer coverage, the intermolecular forces between the coupling agents molecules caused by multi-layer loading are weaker than the direct interaction between the coupling agents and the glass fiber, making it easier to remove by calcination, which could be consistent with the results reported by G. R. Baran *et al.*[34]

Performance of modified GF/PA6 composite material

In order to compare the effects of different types and concentrations of silane coupling agents on the mechanical properties of glass fiber/PA6 composites, the specimens were subjected to mechanical experiment and the tensile stress results of the different specimens are shown in Fig. 6.

From the figure, glass fiber/PA6 composite materials modified with silane coupling agents have showed improved mechanical strength compared with unmodified glass fiber/PA 6 specimens. With the increase of APTES concentration, the tensile stress of glass fiber/PA6 composite specimens shows a trend of increasing firstly and then decreasing. The sample of GF-APTES-1.5/PA6 shows the highest tensile stress of 120 MPa, which is 41% higher than that of unmodified glass fiber/PA6 composite specimens. In contrast, the tensile stress of GF-GBSilane/PA6 specimens were significantly improved. Under the same concentration, the mechanical properties of GF-GBSilane/PA6 specimens were higher that those of GF-APTES/PA6 specimens. Especially, the tensile stress of the GF-GBSilane-1.5/PA6 specimens could reach up to 142 MPa, which has increased by 67% compared with unmodified glass fiber/PA6 composite material. These improved mechanical properties indicate that two silane coupling agents can enhance the adhesion between the reinforcing glass fiber and the matrix PA6, and GBSilane exhibits a more effective promoting effect, which suggests that GBSilane may provide stronger physico-chemical interaction compared to APTES.

In order to investigate the toughness improvement of glass fiber/PA6 composites treated with different types and concentrations of silane coupling agents, notch impact strength tests were conducted on the as-prepared specimens, and the corresponding results are shown in Fig. 7.

From the figure, the notch impact strength of unmodified glass fiber/PA6 composite material is 5.8 kJ m^{-2}. The notch impact strength of GF-APTES/PA6 specimens shows a trend of

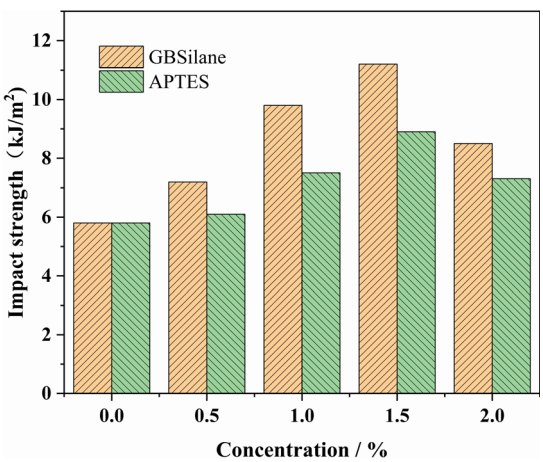

Fig. 7 Notch impact strength of glass fiber/PA6 composite modified with silane coupling agent.

increasing firstly and then decreasing with concentration increasing, indicating that silane coupling agent treatment of glass fiber is beneficial for improving the toughness of glass fiber/PA6 composite material. Under the optimal treatment concentration of 1.5%, the notch impact strength can reach 9.0 kJ m^{-2}, which is 55% higher than that of untreated glass fiber. In contrast, the toughness improvement of GF-GBSilane/PA6 composites is more significant. At the same concentration, the notch impact strength of GF-GBSilane/PA6 is significantly higher than that of GF-APTES/PA6 specimens. Significantly, the notch impact strength of the GF-GBSilane-1.5/PA6 specimens was 11.4 kJ m^{-2}, which was 96.5% higher than that of untreated glass fiber. These results demonstrated that silane coupling agent layer on the glass fiber surface could promote the impact transfer from matrix PA6 to glass fibers. Moreover, GBSilane modification has demonstrated better promotion effect than APTES modification. Totally, the stronger interaction induced by silane coupling agent could inhibit the phase separation, improve tensile stress and impact strength, and contribute to the improved mechanical performances.

Density functional theory calculations

As we know, the hydrogen bonding is difficult to detect through experimental methods. In theoretical simulation software at different scales, DFT can well calculate and simulate physicochemical bonds such as electrostatic interactions, hydrogen bonds, and ionic bonds.[35] To disclose the possible mechanical improvement mechanism of glass fiber/PA6 composite material, this research analyzes the hydrogen bonds, bond length, and binding energy between various silane coupling agents including APTES and GBSilane and PA6 molecules using the Gaussian 16 program. Due to the complexity of polymer materials and the fact that DFT calculation methods can only calculate models with a limited number of atoms, 6-propamidohexanoic acid acetamide was used as the model repeating unit of PA6 polymer, which can fully demonstrate the chemical bonds that can generate hydrogen bonding in PA6 molecules. Meanwhile, compared to PA6 molecules, the molecules number of silane coupling agents is very small. Regardless of the modification ratio, silane coupling agent molecules are surrounded by a large number of PA6 molecules. Therefore, from the perspective of theoretical simulation, the hydrogen bonding calculation between a single PA6 model and a single silane coupling agent molecule can clarify the mode and strength of the interaction, which is also advantageous in terms of DFT calculation. The initial state of PA6 and silane coupling agent molecular simulation is set to approximate the PA6 amide chain to the $-NH_2$ of APTES or the amide structure of GBSilane molecules, and the binding state of its lowest energy state is calculated through software. Fig. 8 has showed the optimized configurations of APTES, GBSilane and PA6 molecules, along with the typical hydrogen bonds between silane coupling agent and PA6, including PA6–APTES and PA6–GBSilane. Based on the calculation results, the overall hydrogen bond number and bond lengths are summarized in Table 1.

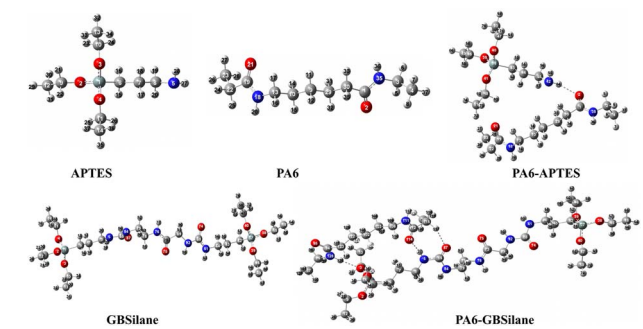

Fig. 8 Optimized molecular configuration of APTES, PA6 and GBSilane, along with hydrogen bonds information between PA6–APTES and PA6–GBSilane.

As illustrated in Fig. 8 and Table 1, APTES could form one hydrogen bond with PA6, as N42–H64···O2(2.17 Å). In comparison, GBSilane could form three hydrogen bonds with PA6, namely C115–H117···O87 (2.45 Å), N5–H27···O114 (1.86 Å) and N128–H129···O3 (2.16 Å).

As we know, hydrogen bond can enhance the mechanical properties of natural composite materials. The excellent mechanical properties of natural wood cellulose and organic–inorganic composite materials such as teeth and bones are closely related to the strong hydrogen bonding between the matrix material and the reinforcing material.[24–26] In general, a shorter bond length of hydrogen bond results in a stronger binding energy, indicating a more stable hydrogen bond formation. From Table 1, the average hydrogen bond length of PA6–APTES is 2.17 Å, and the average hydrogen bond length of PA6–GBSilane is 2.16 Å. The increased hydrogen bond number and decreasing bond length of PA6–GBSilane suggests that there is a stronger interaction between GBSilane and PA6 through hydrogen bond than APTES.

According to the DFT calculation results, the binding energy was expressed as the electronic energy difference between PA6–APTES/GBSilane and PA6 plus APTES/GBSilane, and the corresponding results have been listed in Table 2.

Table 1 Hydrogen bond information summary of PA6–APTES and PA6–GBSilane

	PA6–APTES	PA6–GBSilane
Hydrogen bond number	1	3
Hydrogen bond information (bond length/Å)	N42–H64···O2(2.17)	C115–H117···O87(2.45) N5–H27···O114(1.86) N128–H129···O3(2.16)
Average bond length/Å	2.17	2.16

Table 2 Electronic energy, binding energy and difference of binding energy of PA6–APTES and PA6–GBSilane

	Electronic energy (Hartree)	Electronic energy (kJ mol^{-1})	Binding energy (kJ mol^{-1})
PA6	−692.45	-1.82×10^6	—
APTES	−926.89	-2.43×10^6	—
GBSilane	−2476.66	-6.50×10^6	—
PA6–APTES	−1619.36	-4.25×10^6	30.90
PA6–GBSilane	−3169.13	-8.32×10^6	58.20

The binding energy of PA6–GBSilane is 58.20 kJ mol^{-1}, significantly higher than PA6–APTES (30.90 kJ mol^{-1}). The calculation results demonstrate that GBSilane could provide much stronger attraction induced by more and stronger hydrogen bond between glass fiber and PA6 than APTES, which could contribute to the improved mechanical performance of GF-GBSilane/PA6 composite materials than GF-APTES/PA6 materials as presented in Fig. 6 and 7.

Discussion on interface mechanism

The literature results indicate that the failure of fiber-reinforced composite materials often occurs at the interface,[36] and glass fibers treated with silane coupling agents to improve their properties is a commonly used method. Based on the structure of silane coupling agents and the mechanical properties of composite materials, various theoretical systems have been formed, such as chemical bond theory, reversible hydrolysis theory, diffusion and permeation network theory, plastic deformation layer theory, *etc.*[37] When the surface of glass fibers is not treated, the functional groups on the surface of glass fibers are mainly polar groups such as Si–O–Si, while the molecular chain structure of PA6 is mainly composed of –CO–NH–(CH_2)– repeating structural units, with tightly stacked molecular chains. The lower compatibility between polyamide chains and the surface of glass fibers induced poor mechanical properties of composite materials.[34] Based on the experimental and DFT calculation results, we believe that the improvement of mechanical properties of glass fiber/PA6 composites treated with GBSilane coupling agents may be beneficial from two aspects. Firstly, the unique bilateral siloxane structure of GBSilane coupling agents could mainly proceed hydrolysis and condensation with Si–OH on the surface of glass fibers, and form stronger chemical bonds with the surface of glass fibers, avoiding the shortcomings of APTES coupling agents that have fewer chemical bonds and lower bonding strength with the surface of glass fibers. Secondly, physico-chemical interactions provide also a more critical role. Specifically, the hydrogen bond between coupling agents and PA6 could contribute significantly to the improved mechanical performance. According to the DFT calculation, one GBSilane molecule can form three hydrogen bonds with one PA6 model, while one APTES molecule can only form one hydrogen bond with PA6 model. More hydrogen bonds enhances the interaction between GF-GBSilane and PA6. In addition, comparing with APTES, there are three amide bonds in the GBSilane structure, similar to PA6 main chain, which could improve the wettability and bonding strength between the substrate material PA6 and the modified glass fiber surface.[38] Meanwhile, the hydrogen bond binding energy between GBSilane and PA6 is as high as 58.20 kJ mol^{-1}, which is nearly twice as much as the corresponding value between APTES and PA6. According to the literature results, the hydrogen bond network between the reinforcing fibers and the matrix material plays a crucial role in stress transfer.[21] When the material is under stress, stress is transmitted to the glass fiber surface through the hydrogen bond network, thus exhibiting improved macroscopic mechanical properties of GF-GBSilane reinforcing PA6 composites, including tensile strength and impact strength.

Conclusions

In conclusion, a kind of novel glycine bridged silane coupling agents has been synthesized and used to treat glass fibers, and the treated glass fibers were used to reinforce polyamide 6. The results showed that the GF-GBSilane/PA6 could yield superior mechanical properties comparing with GF-APTES/PA6. Comparing with glass fibers without modification, the modified GF-GBSilane-1.5/PA6 has demonstrated the improved mechanical properties by 67% and 96.5% in respective tensile strength and notch impact strength. In comparison, the corresponding properties of the modified GF-APTES-1.5/PA6 could be increased by 41% and 55%, respectively. DFT results indicate that the stronger hydrogen bond is formed between GBSilane and PA6 than APTES, which have produced the stronger PA6–GBSilane binding energy of 58.20 kJ mol^{-1}. By comparison, the binding energy of PA6–APTES is only 30.90 kJ mol^{-1}. These results demonstrated that the high hydrogen bond density of silane coupling agents would improve interphase adhesion through hydrogen bond mechanism and successively improve the mechanical properties. These findings would provide ideas for the design of efficient silane coupling agents for composite materials.

Data availability

The authors confirm that the data supporting the findings of this study are available within the article.

Author contributions

Dinghua Yu: supervision, data curation, project administration, writing – review & editing. Jianqiang Wang: data acquirement, methodology, investigation. Guowei Wang: density functional theory calculations.

Conflicts of interest

The authors declare that they have no known competing financial interests or personal relationships that could have appeared to influence the work reported in this paper.

Acknowledgements

This work was supported by the open research funding of Ningbo Polytechnic China Light Industry Plastic Mold Engineering Technology Research Center (No. NZ23KF03).

Notes and references

1 B. De, M. Bera, D. Bhattacharjee, B. C. Ray and S. Mukherjee, *Prog. Mater. Sci.*, 2024, **146**, 101326.
2 P. Morampudi, K. K. Namala, Y. K. Gajjela, M. Barath and G. Prudhvi, *Mater. Today: Proc.*, 2021, **43**, 314–319.
3 Y. Zhou, S. Jeelani and T. Lacy, *J. Compos. Mater.*, 2014, **48**, 3659–3672.
4 H. Takagi, *Adv. Compos. Mater.*, 2019, **28**, 525–543.
5 S. Sasidharan and A. Anand, *Ind. Eng. Chem. Res.*, 2020, **59**, 12617–12631.
6 A. Kausar, *Adv. Mater. Sci.*, 2019, **19**, 67–82.
7 B. Azzopardi, A. Hapid, S. Kaleg, D. Onggo and A. C. Budiman, *Energies*, 2023, **16**, 6223.
8 V. E. Ogbonna, P. I. Popoola, O. M. Popoola and S. O. Adeosun, *Eng. Failure Anal.*, 2022, **138**, 106369.
9 D. S. Cousins, Y. Suzuki, R. E. Murray, J. R. Samaniuk and A. P. Stebner, *J. Cleaner Prod.*, 2019, **209**, 1252–1263.
10 D. Kang, S. Yun and B. K. Kim, *Energies*, 2022, **15**, 4357.
11 P. Jagadeesh, M. Puttegowda, O. P. Oladijo, C. W. Lai, S. Gorbatyuk, D. Matykiewicz, S. M. Rangappa and S. Siengchin, *Polym. Compos.*, 2022, **43**, 1238–1251.
12 C. Soutis, *Prog. Aerosp. Sci.*, 2005, **41**, 143–151.
13 J. K. Kocsis, H. Mahmood and A. Pegoretti, *Prog. Mater. Sci.*, 2015, **73**, 1–43.
14 S. Huang, Q. Fu, L. Yan and B. Kasal, *J. Mater. Res. Technol.*, 2021, **13**, 1441–1484.
15 L. Chen, H. Jin, Z. Xu, M. Shan, X. Tian, C. Yang, Z. Wang and B. Cheng, *Mater. Chem. Phys.*, 2014, **145**, 186–196.
16 L. Chen, H. Jin, Z. Xu, J. Li, Q. Guo, M. Shan, C. Yang, Z. Wang, W. Mai and B. Cheng, *J. Mater. Sci.*, 2015, **50**, 112–121.
17 P. Feng, L. Ma, G. Wu, X. Li, M. Zhao, L. Shi, M. Wang, X. Wang and G. Song, *Compos. Sci. Technol.*, 2020, **200**, 108336.
18 S. Kumar, G. Graninger, S. C. Hawkins and B. G. Falzon, *Composites, Part A*, 2021, **148**, 106475.
19 L. Mao, H. Gao, H. Yao, L. Liu, H. Cölfen, G. Liu, S. Chen, S. Li, Y. Yan, Y. Liu and S. Yu, *Science*, 2016, **354**, 107–110.
20 C. Zhao, P. Zhang, J. Zhou, S. Qi, Y. Yamauchi, R. Shi, R. Fang, Y. Ishida, S. Wang, A. P. Tomsia, M. Liu and L. Jiang, *Nature*, 2020, **580**, 210–215.
21 H. Li, C. Liu, J. Zhu, J. Sun, X. Huan, H. Geng, T. Li, L. Ge, X. Jia, X. Yang and H. Wang, *Composites, Part B*, 2024, **280**, 111476.
22 H. Li, C. Liu, J. Zhu, X. Huan, P. Qi, K. Xu, H. Geng, X. Guo, H. Wu, L. Zu, L. Ge, X. Jia, X. Yang and H. Wang, *Adv. Compos. Hybrid Mater.*, 2024, **7**, 72.
23 H. S. Gupta, S. Krauss, M. Kerschnitzki, A. Karunaratne, J. W. C. Dunlop, A. H. Barber, P. Boesecke, S. S. Funari and P. Fratzl, *J. Mech. Behav. Biomed. Mater.*, 2013, **28**, 366.
24 G. E. Fantner, T. Hassenkam, J. H. Kindt, J. C. Weaver, H. Birkedal, L. Pechenik, J. A. Cutroni, G. A. G. Cidade, G. D. Stucky, D. E. Morse and P. K. Hansma, *Nat. Mater.*, 2005, **4**, 612.
25 K. J. Koester, J. W. Ager and R. O. Ritchie, *Nat. Mater.*, 2008, **7**, 672.
26 M. E. Launey, M. J. Buehler and R. O. Ritchie, *Annu. Rev. Mater. Res.*, 2010, **40**, 25.
27 J. H. Lee, K. Y. Rhee and S. J. Park, *Composites, Part A*, 2011, **42**, 478–483.
28 J. Wang, W. Zhang, C. Gu, W. Zhang, M. Zhou, Z. Wang, C. Guo and L. Sun, *Chem.–Asian J.*, 2017, **12**, 3162–3171.
29 J. Wang, M. Zhou, C. Gu, W. Zhang, M. Lv, C. Guo, L. Sun and H. Zhang, *Mater. Lett.*, 2017, **193**, 299–304.
30 J. Wang, C. Gu, M. Zhou, W. Zhang, Z. Wang, M. Lv, C. Guo and L. Sun, *Micro Nano Lett.*, 2017, **12**, 1006–1010.
31 L. Sang, Y. Wang, G. Chen, J. Liang and Z. Wei, *RSC Adv.*, 2016, **6**, 107739–107747.
32 M. J. Frisch, G. W. Trucks, H. B. Schlegel, G. E. Scuseria, M. A. Robb, J. R. Cheeseman, G. Scalmani, V. Barone, G. A. Petersson, H. Nakatsuji, X. Li, M. Caricato, A. V. Marenich, J. Bloino, B. G. Janesko, R. Gomperts, B. Mennucci, H. P. Hratchian, J. V. Ortiz, A. F. Izmaylov, J. L. Sonnenberg, D. Williams-Young, F. Ding, F. Lipparini, F. Egidi, J. Goings, B. Peng, A. Petrone, T. Henderson, D. Ranasinghe, V. G. Zakrzewski, J. Gao, N. Rega, G. Zheng, W. Liang, M. Hada, M. Ehara, K. Toyota, R. Fukuda, J. Hasegawa, M. Ishida, T. Nakajima, Y. Honda, O. Kitao, H. Nakai, T. Vreven, K. Throssell, J. A. Montgomery Jr, J. E. Peralta, F. Ogliaro, M. J. Bearpark, J. J. Heyd, E. N. Brothers, K. N. Kudin, V. N. Staroverov, T. A. Keith, R. Kobayashi, J. Normand, K. Raghavachari, A. P. Rendell, J. C. Burant, S. S. Iyengar, J. Tomasi, M. Cossi, J. M. Millam, M. Klene, C. Adamo, R. Cammi, J. W. Ochterski, R. L. Martin, K. Morokuma, O. Farkas, J. B. Foresman and D. J. Fox, *Gaussian 16, Revision B.01*, Gaussian, Inc., Wallingford CT.
33 H. Zheng, H. He, M. Lu, Y. Pei, H. Peng, W. Zhou, C. Guo and J. Wang, *Microporous Mesoporous Mater.*, 2024, **373**, 113133.
34 S. Debnath, S. L. Wunder, J. I. Mccool and G. R. Baran, *Dent. Mater.*, 2003, **19**, 441–448.
35 B. G. Janesko, *Chem. Soc. Rev.*, 2021, **50**, 8470–8495.
36 H. Wu, D. W. Dwight and N. T. Huff, *Compos. Sci. Technol.*, 1997, **57**, 975–983.
37 Y. Wang, C. J. Hansen, I. M. McAninch, E. J. Robinette and A. M. Peterson, *ACS Appl. Polym. Mater.*, 2022, **4**, 4244–4253.
38 Y. Wang, C. J. Hansen, C. C. Wu, E. J. Robinette and A. M. Peterson, *RSC Adv.*, 2021, **11**, 31142–31151.